

Entanglement production by independent quantum channels

Örs Legeza^{1,2}, Florian Gebhard¹, Jörg Rissler¹

¹*Fachbereich Physik, Philipps-Universität Marburg, D-35032 Marburg, Germany*

²*Research Institute for Solid-State Physics and Optics, H-1525 Budapest, Hungary*

For the one-dimensional Hubbard model subject to periodic boundary conditions we construct a unitary transformation between basis states so that open boundary conditions apply for the transformed Hamiltonian. Despite the fact that the one-particle and two-particle interaction matrices link nearest and next-nearest neighbors only, the performance of the density-matrix renormalization group method for the transformed Hamiltonian does not improve. Some of the new interactions act as independent quantum channels which generate the same level of entanglement as periodic boundary conditions in the original formulation of the Hubbard model. We provide a detailed analysis of these channels and show that, apart from locality of the interactions, the performance of DMRG is effected significantly by the number and the strength of the quantum channels which entangle the DMRG blocks.

PACS numbers: 03.67.-a, 71.10.Fd

I. INTRODUCTION

The numerical density-matrix renormalization group (DMRG) method¹ works best for lattice models with short-range interactions and open boundary conditions. Non-localized versions have become a major field of research, e.g., the DMRG in momentum space^{2,3,4} and in quantum chemistry^{5,6,7,8,9,10}. For these applications, it is well established that the ordering of ‘lattice sites’ and the proper choice of basis states crucially influence the convergence properties of the DMRG algorithm; for a review, see Refs. [11,12,13,14]. When Chan and Head-Gordon applied a quantum-chemistry version of the DMRG (QC-DMRG) to the calculation of the ground-state energy of selected molecules⁶, they found that the DMRG leads to significantly better results when lattice sites are re-ordered with the help of the Cuthill–McKee algorithm¹⁵. However, using concepts inherited from quantum information theory, it has been shown that the Cuthill–McKee algorithm fails to generate an optimal ordering in general⁴. In fact, it can lead to very bad configurations which may even prevent the DMRG algorithm from converging to the proper ground-state energy.

The accuracy and convergence of the DMRG for given computer resources is intimately related to the entanglement of the DMRG blocks during the renormalization group step. Therefore, the von-Neumann entropy of the blocks can be used to optimize the required computational resources^{4,16}. The generation of block entropy as a function of system size was studied in detail by various groups^{17,18}. Recently, the entropy-approach was extended in [19] to include the two-site entropy profile. It suggests a way to improve the criteria for the generation of basis states and a proper ordering of the corresponding ‘lattice sites’. The study of various orderings by brute-force algorithms confirmed the best orderings as found from entropy-based methods but no definite conclusions could be reached yet²⁰.

For lattice models, boundary conditions also have a strong influence on the performance of the DMRG algo-

rithm. When periodic instead of open boundary conditions are used for the one-dimensional Hubbard model, the block entropy increases significantly with system size¹⁶. In order to reduce numerical efforts to solve problems subject to periodic boundary conditions, the matrix-product state description has been introduced, for which, however, the interaction matrices become less sparse, and, thus, a true gain in performance could not be documented yet²¹. Recent studies^{16,22} indicate that entanglement localization and interaction localization actually compete and should be treated on an equal footing. The central goal remains the development of a standard procedure to find a basis state transformation for a given model which minimizes the block entanglement and thereby optimizes the performance of the DMRG algorithm in terms of required computational resources for a given demand on accuracy.

In this work we introduce a unitary basis transformation for the one-dimensional Hubbard model with periodic boundary conditions which results in a two-chain geometry with open boundary conditions and couplings between nearest neighbors and next-nearest neighbors only. Contrary to expectation, the performance of the DMRG algorithm does not improve. Our analysis shows that the transformation opens new quantum channels which interfere with the kinetic-energy channel and lead to a substantial entanglement between the DMRG blocks.

We organize our paper as follows. In section II we describe briefly the Hubbard Hamiltonian and the unitary transformation to the two-chain geometry with localized interactions and open boundary conditions. In section III we discuss our numerical procedure with an emphasis on the control of accuracy and the data analysis. We present our numerical DMRG results in section IV. We find that the DMRG procedure is more efficient for the Hubbard model with periodic boundary conditions than for the transformed version with open boundary conditions. We analyze this result in terms of the influence of independent quantum channels in section V. In particular, we show that a super-site representation for the two-chain

geometry does not remedy the basic entanglement problem of competing quantum channels. We draw our conclusions in section VI.

II. BASIS STATE TRANSFORMATION

A. Hubbard model

We consider the one-dimensional Hubbard model with uniform nearest-neighbor hopping on a finite chain of L_s lattice sites subject to periodic boundary conditions,

$$\begin{aligned}\hat{H} &= -t\hat{H}_T + U\hat{H}_U \\ \hat{H}_T &= \sum_{j=0, \sigma}^{L_s-1} (\hat{c}_{j, \sigma}^+ \hat{c}_{j+1, \sigma} + \hat{c}_{j+1, \sigma}^+ \hat{c}_{j, \sigma}) , \\ \hat{H}_U &= \sum_{j=0}^{L_s-1} \hat{n}_{j, \uparrow} \hat{n}_{j, \downarrow} ,\end{aligned}\quad (1)$$

where $\hat{c}_{j, \sigma}^+$ ($\hat{c}_{j, \sigma}$) is the creation (annihilation) operator for electrons with spin $\sigma = \uparrow, \downarrow$ at site j , $\hat{n}_{j, \sigma} = \hat{c}_{j, \sigma}^+ \hat{c}_{j, \sigma}$, and $\hat{n}_j = \hat{n}_{j, \uparrow} + \hat{n}_{j, \downarrow}$ is the occupation number at site j . Due to periodic boundary conditions we set $\hat{c}_{L_s, \sigma} \equiv \hat{c}_{0, \sigma}$.

The single-particle interaction matrix is given by \hat{H}_T . We use the intersite hopping parameter t as unit of energy and set to $t = 1$ in the following. The two-particle interaction is given by \hat{H}_U and U is the strength of the on-site Coulomb interaction. The schematic plot of the model for a chain with $L_s = 10$ lattice sites with periodic boundary conditions is shown in Fig. 1.

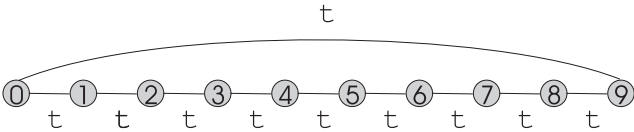


FIG. 1: Schematic plot of the Hubbard model with periodic boundary conditions for a chain with $L_s = 10$ lattice sites. Solid lines denote the nearest-neighbor hopping while the on-site Coulomb interaction is shown by the gray shading. Numbers indicate the lattice site indices.

It is evident from Fig. 1 and eq. (1) that the single-particle and the two-particle interaction matrices are diagonally dominated apart from the fact that \hat{H}_T has two off-diagonal terms due to the couplings between sites $j = 0$ and $j = L_s - 1$ when periodic boundary conditions are employed. These two terms leads to an enlarged bandwidth of \hat{H}_T and to a larger entanglement in the system as compared to the case of open boundary conditions. Therefore, we should find a transformation which reduces the bandwidth of \hat{H}_T . A reordering of lattice sites cannot lead to more localized interactions as will be shown in section IV. Thus, we need to apply an appropriate unitary transformation to new basis states.

B. Two-chain geometry

Let us define the following unitary transformation for an even number of lattice sites,

$$\begin{aligned}\hat{a}_{0, \sigma} &\equiv \hat{c}_{0, \sigma} , \quad \hat{a}_{L_s/2, \sigma} \equiv \hat{c}_{L_s/2, \sigma} , \\ \hat{a}_{j, \sigma} &\equiv \sqrt{\frac{1}{2}} (\hat{c}_{j, \sigma} + \hat{c}_{L_s-j, \sigma}) \quad \text{for } j = 1, 2, \dots, \frac{L_s}{2} - 1 , \\ \hat{b}_{j, \sigma} &\equiv \sqrt{\frac{1}{2}} (\hat{c}_{j, \sigma} - \hat{c}_{L_s-j, \sigma}) \quad \text{for } j = 1, 2, \dots, \frac{L_s}{2} - 1 .\end{aligned}\quad (2)$$

The back-transformation reads for $j = 1, 2, \dots, L_s/2 - 1$

$$\begin{aligned}\hat{c}_{j, \sigma} &\equiv \sqrt{\frac{1}{2}} (\hat{a}_{j, \sigma} + \hat{b}_{j, \sigma}) , \\ \hat{c}_{L_s-j, \sigma} &\equiv \sqrt{\frac{1}{2}} (\hat{a}_{j, \sigma} - \hat{b}_{j, \sigma}) .\end{aligned}\quad (3)$$

The transformation is the result of a Lánczos basis representation of the kinetic energy which starts from the state $|\Phi_0\rangle = \hat{c}_{0, \sigma}^+ |\text{vac}\rangle$. In this way, all the operators $\hat{a}_{j, \sigma}$ are generated. The operators $\hat{b}_{j, \sigma}$ naturally follow as the antisymmetric linear combinations of the operators $\hat{c}_{j, \sigma}$ and $\hat{c}_{L_s-j, \sigma}$.

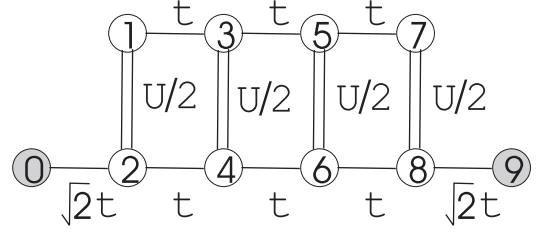


FIG. 2: Schematic plot of the transformed Hubbard model using the unitary transformation (2). Single solid lines denote single-particle couplings, double solid lines correspond to two-particle interactions. Shaded circles denote the on-site Coulomb interaction of strength U while empty circles correspond to strength $U/2$. Numbers indicate the lattice site indices.

In terms of the new operators the kinetic energy becomes

$$\begin{aligned}\hat{H}_T &= \sum_{\sigma} \sqrt{2} \left[\hat{a}_{0, \sigma}^+ \hat{a}_{1, \sigma} + \hat{a}_{L_s/2, \sigma}^+ \hat{a}_{L_s/2-1, \sigma} + \text{h.c.} \right] \\ &+ \sum_{j=1, \sigma}^{L_s/2-2} \left[\hat{a}_{j, \sigma}^+ \hat{a}_{j+1, \sigma} + \hat{b}_{j, \sigma}^+ \hat{b}_{j+1, \sigma} + \text{h.c.} \right] .\end{aligned}\quad (4)$$

The geometry of the transformed model is shown schematically in Fig. 2. As seen from the figure, the transformed model displays a two-chain geometry with open boundary conditions. Moreover, the kinetic energy only couples nearest-neighbor sites of type a or b . Thus, \hat{H}_T

is diagonally dominated as for the case of the Hubbard model with open boundary conditions.

When we apply the unitary transformation to the two-particle interaction matrix we find

$$\hat{H}_U = n_{0,\uparrow}^a n_{0,\downarrow}^a + n_{L_s/2,\uparrow}^a n_{L_s/2,\downarrow}^a + \frac{1}{2} [\hat{H}_{U,d} + \hat{H}_{U,p} + \hat{H}_{U,s}] \quad (5)$$

with the local direct, pair-hopping, and spin-flip terms

$$\begin{aligned} \hat{H}_{U,d} &= \sum_{j=1}^{L_s/2-1} (n_{j,\uparrow}^a + n_{j,\uparrow}^b) (n_{j,\downarrow}^a + n_{j,\downarrow}^b), \\ \hat{H}_{U,p} &= \sum_{j=1}^{L_s/2-1} \left(\hat{a}_{j,\uparrow}^+ \hat{b}_{j,\uparrow} \hat{a}_{j,\downarrow}^+ \hat{b}_{j,\downarrow} + \hat{b}_{j,\uparrow}^+ \hat{a}_{j,\uparrow} \hat{b}_{j,\downarrow}^+ \hat{a}_{j,\downarrow} \right), \\ \hat{H}_{U,s} &= \sum_{j=1}^{L_s/2-1} \left(\hat{a}_{j,\uparrow}^+ \hat{b}_{j,\uparrow} \hat{b}_{j,\downarrow}^+ \hat{a}_{j,\downarrow} + \hat{b}_{j,\uparrow}^+ \hat{a}_{j,\uparrow} \hat{a}_{j,\downarrow}^+ \hat{b}_{j,\downarrow} \right). \end{aligned} \quad (6)$$

The schematic plot of the two-particle interaction is also shown in Fig. 2. It is evident that we have transformed the Hubbard model with periodic boundary conditions into a two-band problem with purely local interactions and nearest-neighbor electron transfers.

C. One-dimensional representation

The standard DMRG algorithm applies to one-band, i.e., single-chain geometries. By ordering the sites of the two-chain geometry next to each other, the Hamiltonian of the transformed model takes the form as shown in Fig. 3. The single-particle interaction matrix contains couplings between next-nearest neighbors. The two-particle interaction matrices contain on-site contributions via the direct term $\hat{H}_{U,d}$, and nearest-neighbor interactions from $\hat{H}_{U,d}$, the pair-hopping term $\hat{H}_{U,p}$, and the spin-flip term $\hat{H}_{U,s}$. Nevertheless, all couplings remain local and the model is subject to open boundary conditions. Therefore, we may expect that we can calculate ground-state properties more efficiently in this formulation than we can for the Hubbard model (1) with periodic boundary conditions.

III. NUMERICAL PROCEDURE

A. Controlling accuracy

As in previous work^{8,16}, we use the dynamic block state selection (DBSS) procedure to control the numerical accuracy of the DMRG method for different models. When we apply the DMRG to the Hubbard model (1) with periodic boundary condition and the transformed model in the one-dimensional geometry of Fig. 3, we fix the quantum information loss (χ) which is closely related to the

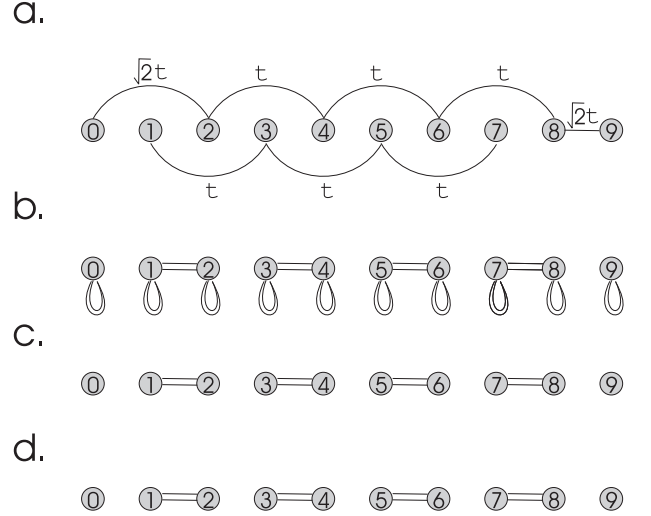


FIG. 3: One-dimensional representation of the single-particle electron transfers \hat{H}_T (a) and the two-particle interactions $\hat{H}_{U,d}$ (b), $\hat{H}_{U,p}$ (c), $\hat{H}_{U,s}$ (d) of the transformed Hubbard model. Loops in figure (b) denote on-site interactions.

relative error of the energy of the target state. In this way, the block entropy as one of the most relevant DMRG performance parameters can be monitored for different model Hamiltonians.

We choose χ to make sure that the maximum number of block states ($M_{\max} \simeq 3000$) that our program can handle is not reached during the calculations, i.e., we do not introduce an additional quantum information loss besides the truncation procedure based on χ . We choose a small minimum number of block states M_{\min} in order to make sure that its specific choice has negligible consequences and yet ensures a reliable data analysis. We use the entropy sum-rule as a criterion of convergence¹⁶. In general, five or six sweeps are carried out in order to make sure that the desired accuracy determined by χ has been reached.

B. Performance monitoring

A natural quantity to measure the DMRG performance would be the CPU time. The CPU time, however, strongly depends on the CPU in use and a number of other technical issues. A software-related quantity to monitor is the block entropy since it determines the number of blocks states required to reach the desired accuracy for the given model and, thus, the speed of the DMRG calculations.

In this work we follow notations introduced in Refs. [4, 16, 19]. We decompose the total system into four subsystems. There are two sites, denoted by s_l and s_r , with q_l and q_r degrees of freedom between the left and right blocks, B_l and B_r , of dimensions M_l and M_r , respectively. The blocks $B_L = B_l \bullet$, $B_R = \bullet B_r$ have dimension M_L and

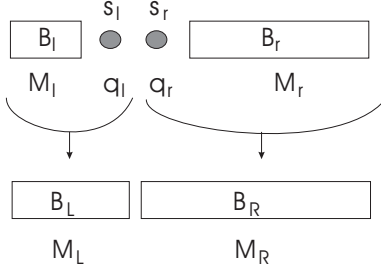


FIG. 4: Schematic plot of the system and environment block of DMRG. B_l and B_r denote the left and right blocks of length l and r , and of dimension M_l and M_r , respectively, where \bullet stands for the intermediate sites (s_l and s_r) with q_l and q_r degrees of freedom. The blocks $B_L = B_l \bullet$ and $B_R = \bullet B_r$ have dimensions M_L and M_R , respectively.

M_R , respectively. This configuration is shown in Fig. 4.

The block entropies are denoted by S_l , S_L , S_r , and S_R . They, as well as the site entropies S_{s_l} and S_{s_r} , are calculated from the respective reduced subsystem density matrices ρ as $S = -\text{Tr} \rho \ln \rho$. The number of degrees of freedom per site, $q_l = q_r \equiv q$, is $q = 4$ for the Hubbard model and the transformed Hubbard model.

Apart from the entropies we monitor the Schmidt number (γ) which counts the number of nonzero eigenvalues of the reduced subsystem density matrix for each superblock partitioning,

$$|\Psi_T\rangle = \sum_{i=1}^{\gamma \leq \min(M_L, M_R)} \omega_i |\Psi_i^{(L)}\rangle \otimes |\Psi_i^{(R)}\rangle, \quad (7)$$

where $|\Psi_T\rangle$ is the wave function of the total system, $|\Psi_i^{(L)}\rangle$ and $|\Psi_i^{(R)}\rangle$ are bi-orthogonal basis states for the left and right blocks with the condition $\sum_i \omega_i^2 = 1$. The Schmidt number provides information about the entanglement of the subsystems when a pure target state is considered. In our numerical analysis we determine γ for a given quantum information loss χ and we demand $\omega_i > 10^{-15}$ when we determine γ . Imposing this cut-off value induces some minor fluctuations in the Schmidt number as a function of the strength of the quantum channels.

C. Total quantum information

In order to compare more rigorously the various representations of a quantum system, we measure the total quantum information, I_{tot} , encoded in the wave function. To this end, we form all system blocks which contain $M_l = 1$ to $M_l = L_s$ lattice sites and sum up the quantum information gain of each renormalization group step¹⁶. If no truncation is applied, I_{tot} also equals the sum of the lattice-site entropies, i.e., $I_{\text{tot}} = \sum_j S_{s_j}$. When we use the DBSS approach the error in I_{tot} is proportional to $L_s \chi$.

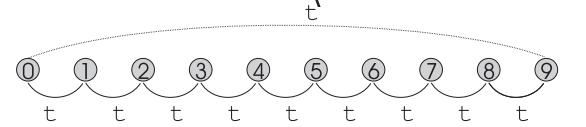
IV. RESULTS FROM DMRG

Let $E(L_s, N_\uparrow, N_\downarrow, U)$ denote the exact ground-state energy of the one-dimensional Hubbard model for a finite chain with L_s lattice sites and N_σ electrons with spin σ as a function of the interaction strength U . It can be obtained from the Bethe Ansatz²³. In this work we study the paramagnetic half-filled case, $N_\uparrow = N_\downarrow = L_s/2$ as a function of U for system sizes $L_s \leq 64$. All numerical data presented are from the results of the last DMRG sweep.

A. Lattice site reordering

A reordering of lattice sites does not effect the total quantum correlation in the system. Therefore, when the model is solved exactly, I_{tot} is a conserved quantity. The entanglement between the DMRG blocks, however, depends on the number of quantum channels in between them and, thus, the ordering of lattice sites has a major impact on the performance of the DMRG method.

a.



b.

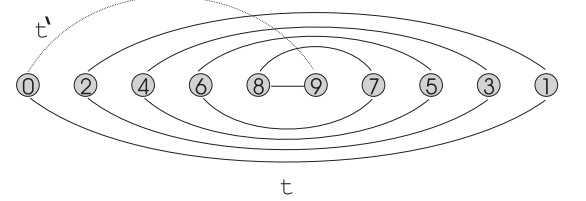


FIG. 5: Two extreme orderings for the Hubbard chain.

For the Hubbard model two extreme configurations are shown in Fig. 5. In Fig. 5 (a) the “communication” between lattice sites $j = 0$ and $j = L_s - 1 = 9$ is mediated by the neighboring lattice sites in between them (strength t) and by a direct channel (strength t'). The worst reordering is shown in Fig. 5 (b) where the total length of all communication paths between lattice sites $j = 0$ and $j = L_s - 1 = 9$ is maximized. In order to quantify these statements we consider the (total) “communication length”,

$$C = \sum_{j=0}^{L_s-1} |\mathcal{P}(j+1) - \mathcal{P}(j)|, \quad (8)$$

where \mathcal{P} permutes the L_s numbers $j = 0, 1, \dots, L_s - 1$ into their new ordering. For example, in Fig. 5 (b) we set $\mathcal{P}_b(0) = 0$, $\mathcal{P}_b(1) = L_s - 1$, $\mathcal{P}_b(2) = 2$, $\mathcal{P}_b(3) =$

$L_s - 2$, and so on. The standard ordering in Fig. 5 (a) amounts to $C^{\text{pbc}}_{\text{link}} = 2(L_s - 1)$ which can not be decreased by any other ordering. For the reordering in Fig. 5 (b), the communication length is $C^{\text{max}}_{\text{link}} = L_s^2/2$.

For a more detailed analysis it is helpful to investigate the number of individual quantum channels between the left and right blocks

$$C_{\text{link}}(l) = \left[\text{sum over all cross-links between } B_L \text{ and } B_R, \text{ where } (l+1) \text{ is the length of } B_L. \right] \quad (9)$$

We have $C^{\text{pbc}}_{\text{link}}(l) = 2$ in the configuration of Fig. 5 (a) whereas $C^{\text{max}}_{\text{link}}(l) = L_s - |2l + 2 - L_s|$ in the configuration of Fig. 5 (b). From the number of quantum channels we define the (total) communication length

$$C = \sum_l C_{\text{link}}(l), \quad (10)$$

which reduces to the expression (8) for our example.

More generally, not only the number but also the strength and the type of the individual quantum channels between the left and right blocks play an important role. In an obvious extension of (10) we may assign adjustable weight factors $\gamma_{\text{channel}}(l, U/t, \dots)$ to each channel. Typically, the communication length C and the number of individual quantum channels at each link $C_{\text{link}}(l)$ are sufficient for a first assessment of the entanglement of the system. The computational cost for one DMRG iteration step is determined by $C_{\text{link}}(l)$ since this number does not depend on the ordering of the lattice sites within the two blocks. The overall cost of a full DMRG sweep, however, also depends on C due to the relationship (10). In future applications, C may serve as a cost function to optimize the ordering (and the basis set).

In Fig. 6 we show the site entropy, the block entropy, and the Schmidt number from exact DMRG calculations for $L_s = 10$ lattice sites at $U = 1$ for the two configurations of Fig. 5. In order to make visible the differences in Schmidt numbers for small system sizes we include results for $\chi = 0$ (exact calculation) and $\chi = 10^{-4}$ with $M_{\text{min}} = 4$. After convergence all lattice sites possess the same entropy, $S_{s_i} \approx 1.377$, and $I_{\text{tot}} \approx 13.77$ is the same for both orderings. However, the block entropy is much larger for the configuration 5 (b), i.e., one needs more computational resources to solve the problem. Correspondingly, the Schmidt number $\gamma(\chi)$ for a given quantum information loss χ is larger for the worst ordering than for the natural ordering. In fact, the block entropy and the Schmidt number closely follow the number of cross-links between the left and right blocks, $C_{\text{link}}(l)$, up to logarithmic corrections in the system size^{17,18}.

There is no site ordering different from the configuration 5 (a) which reduces the number of cross-links below two, $C^{\text{min}}_{\text{link}} = 2$, and the communication length below $C^{\text{min}} = 2(L_s - 1)$. Thus, we conclude that the total quantum correlation in the system cannot be reduced by a reordering of the sites. Only a basis-state transformation might offer a way to achieve the desired entanglement reduction.

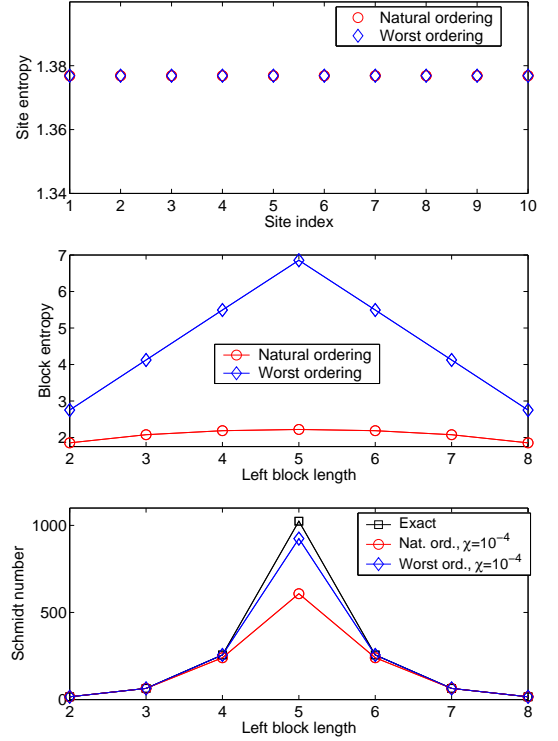


FIG. 6: Site entropy and block entropy for the half-filled Hubbard model for the two ordering criteria shown in Fig. 5 for $U = 1$ and $\chi = 0$ (exact calculation). The Schmidt number is also shown for $\chi = 10^{-4}$ and $M_{\text{min}} = 4$. The lines are guides to the eyes.

B. Basis-state transformation

Since interactions are localized for the transformed Hubbard model we might expect that the entanglement in the system is reduced, and, thus, the problem can be solved more efficiently using DMRG. In Fig. 7 we plot the site entropy, the block entropy, and the Schmidt number for the non-interacting Hubbard model and the transformed model for $\chi = 10^{-4}$, $M_{\text{min}} = 64$, and $L_s = 64$ sites as a function of the number of DMRG sweeps. Note that the limit $U = 0$ poses a non-trivial problem for the position-space DMRG.

For both models we determine the ground-state energy within the desired relative accuracy of better than 10^{-3} . The comparison of data points in Figs. 7 shows, however, that the basis-state transformation (2) did not lead to a significant improvement: the site and block entropies as well as the Schmidt number are only marginally smaller than for the Hubbard model with periodic boundary conditions.

This result can again be understood from the number of cross links and the communication length in Fig. 3 (a). The number of cross links is the same for both representations, $C^{\text{pbc}}_{\text{link}} = C^{\text{transf}}_{\text{link}} = 2$, and the communication length is almost the same, too, $C^{\text{transf}} = 2L_s - 5$ versus $C^{\text{pbc}} = 2L_s - 2$, see section IV A.

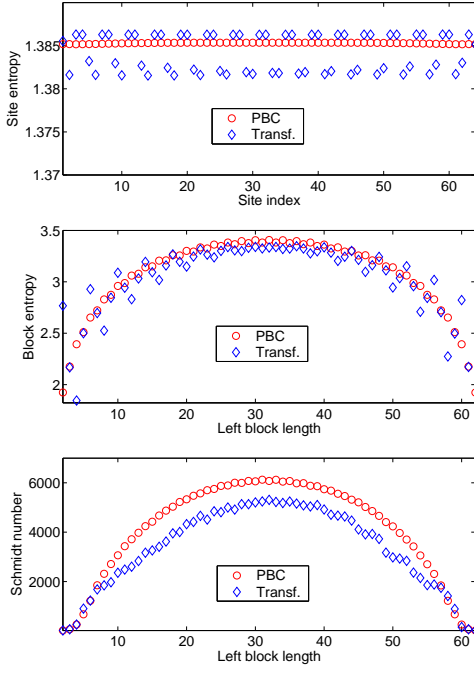


FIG. 7: Same as Fig. 6 for the Hubbard model with periodic boundary conditions and for the transformed Hubbard model with open boundary conditions for $\chi = 10^{-4}$, $M_{\min} = 64$ (PBC) and $M_{\min} = 256$ (Transf.), $L_s = 64$, and $U = 0$.

In order to demonstrate the importance of the number of links and of the communication length, we treat the two chains for a -electrons and b -electrons separately as they decouple for $U = 0$, see Fig. 2. For this geometry, the DMRG result is shown in Fig. 8. The block entropy profile clearly shows the absence of quantum correlations between the two independent chains. For this geometry we have $C_{\text{link}}^{\text{two-chain}}(l) = 1$ for the a -chain and b -chain separately. The communication length for both chains together is $C^{\text{two-chain}} = L_s - 2$. Therefore, it is smaller by a factor of two than for periodic boundary conditions, $C^{\text{PBC}} = 2L_s - 2$. It is evident from Fig. 8 that the maximum of the block entropy has equally dropped by almost a factor of two, from 3.3 for periodic boundary conditions to 1.7 for the two-chain geometry, and the Schmidt number has reduced by more than one order of magnitude.

The situation drastically changes when the Hubbard interaction is switched on. As shown for $U = 10$ in Fig. 9, the site entropy and the block entropy are actually *larger* for the transformed Hubbard model with open boundary conditions so that *more* block states are required to reach the same accuracy as in the original formulation of the Hubbard model with periodic boundary conditions. Note that the oscillation in the block entropy is related to the dimer configuration of the Coulomb interaction, i.e., the number of bonds between DMRG blocks $C_{\text{link}}^{\text{transf}}(l)$ oscillates between two and eight. Therefore, the block entropy of the two representations is the same for every second RG iteration step for which there are only the two t -type channels between the DMRG blocks.

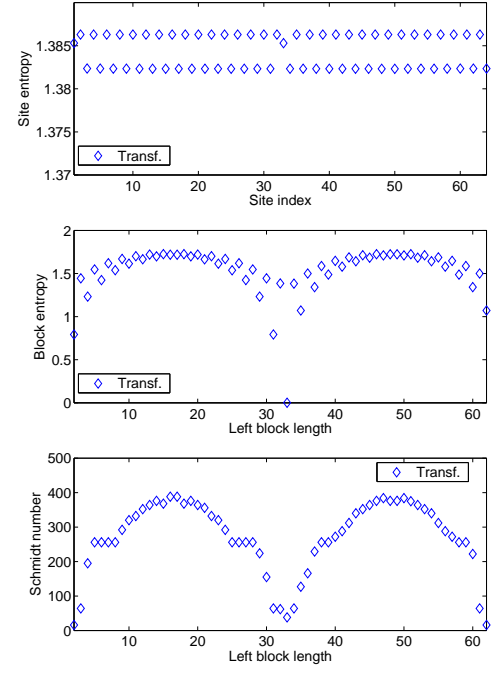


FIG. 8: Same as Fig. 7 for the transformed Hubbard model with open boundary conditions for $U = 0$, $\chi = 10^{-4}$, and $M_{\min} = 64$ in independent-chain geometry.

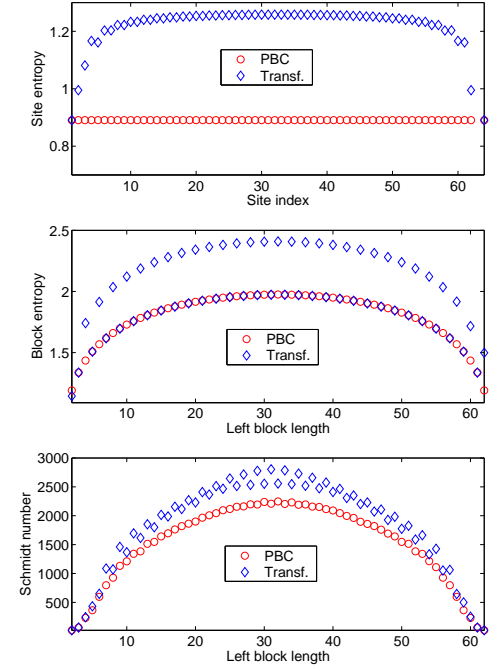


FIG. 9: Same as Fig. 7 for $U = 10$ and $\chi = 10^{-5}$.

As seen from Fig. 10, the total quantum information of the transformed Hubbard model (2) in the geometry of Fig. 2 (a) is smaller than that of the Hubbard model with periodic boundary conditions only for very small values of the interaction strength, $U < \mathcal{O}(t/L_s)$.

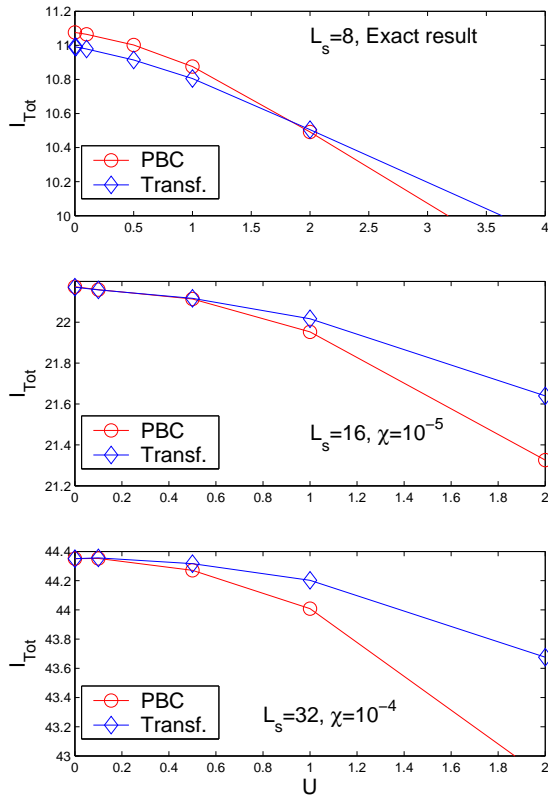


FIG. 10: Total quantum information for the original and transformed Hubbard models as a function of U for various system sizes. For $L_s = 8$ results are exact while for larger system sizes data were obtained by setting $\chi = 10^{-5}$.

Apparently, the interactions of our transformed Hamiltonian, albeit fairly local, generate a strong entanglement between lattice sites and subsystems because they and the kinetic energy act as independent and actually competing quantum channels. We shall investigate this point further in section V. Here, we merely determine the communication length by adding up equally the distances for single-particle and two-particle electron transfers. The terms $\hat{H}_{U,d}$, $\hat{H}_{U,p}$ and $\hat{H}_{U,s}$ contribute equally to give the estimate $C^{\text{transf}} \approx 7L_s/2$. The larger entanglement in the transformed Hubbard model as expressed by $C^{\text{transf}} > C^{\text{pbc}} = 2(L_s - 1)$ implies that the DMRG allocates more computational resources for the transformed Hamiltonian than for the Hubbard model with periodic boundary conditions.

From a technical point of view, the overall CPU time increases by a factor of four to five also because more matrix multiplications are necessary. In contrast to the Hubbard model with periodic boundary conditions, nine matrix multiplications instead of two must be carried out during the superblock diagonalization and three times more operators need to be renormalized. Moreover, due to the new channels and the increase of entanglement in the system, the number of Davidson matrix multiplication increases by a factor of two to three.

V. EFFECTS OF INDEPENDENT QUANTUM CHANNELS

In this section we study the entanglement generation in more detail. To this end, we switch on perturbatively various coupling terms shown in Fig. 3.

A. Smooth interpolation between open and periodic boundary conditions

First, we consider how entanglement between DMRG blocks is generated for the configuration shown in Fig. 5 where we smoothly interpolate between open boundary conditions ($t' = 0$) and periodic boundary conditions ($t' = 1$) as a function of t' for $t = 1$ and $U = 0$. Our results are shown in Fig. 11. The total quantum information, the block entropy and the Schmidt number change smoothly as a function of t' . Thus, the second quantum channel opened by the periodic boundary conditions behaves perturbatively. This is not always the case as seen in the next example. Note, however, that the perturbation leads to a small effect only as long as $t' < \mathcal{O}(t/L_s)$.

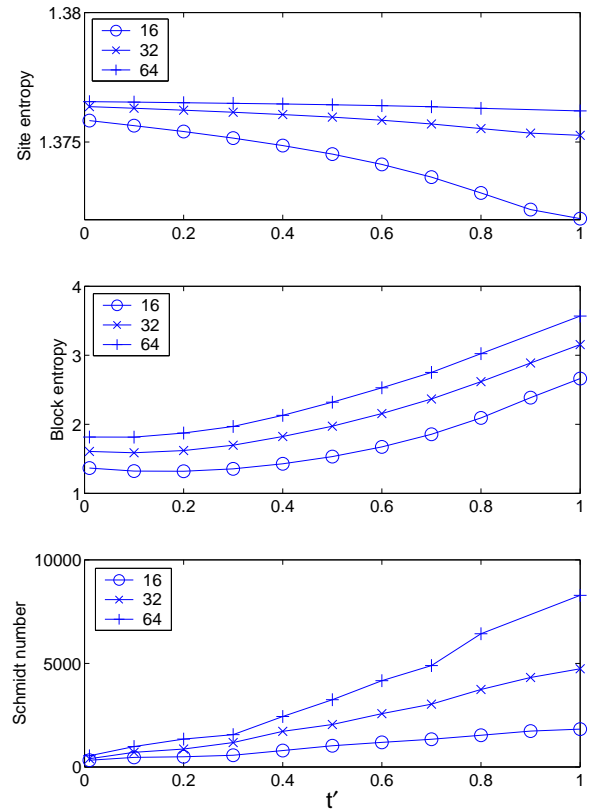


FIG. 11: Site entropy, block entropy, and Schmidt number for the half-filled Hubbard model for the configuration shown in Fig. 5 (a) as a function of t' for $t = 1$ and $U = 0$ for $L_s = 16, 32$ sites, and $\chi = 10^{-4}$, $M_{\min} = 64$.

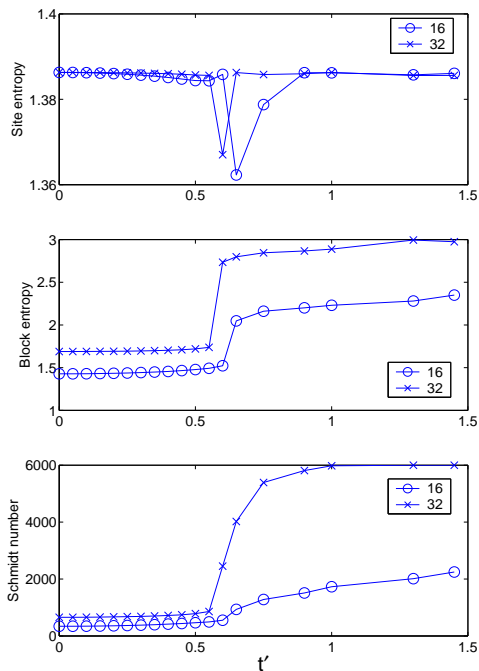


FIG. 12: Same as Fig. 11 for the half-filled Hubbard model with open boundary condition as a function of the transfer integral t' between next-nearest neighbors. We set $t = 1$ and $U = 0$ for $L_s = 16, 32$ and $\chi = 10^{-4}$, $M_{\min} = 64$.

B. Electron transfer between nearest and next-nearest neighbors

Next, we analyze the entropy generation by an additional next-nearest neighbor electron transfer amplitude for the Hubbard model. The nearest-neighbor hopping is again set to $t = 1$ whereas the transfer integral between next-nearest neighbors t' is smoothly increased. As in the previous example we choose $U = 0$ to avoid the effect of other channels. In Fig. 12 we plot the site entropy, the block entropy and the Schmidt number as a function of t' . These quantities change smoothly as a function of t' up to a critical value where they increase rapidly. The value for the rapid increase coincides with the metal-insulator transition point in the t - t' - U model, see, e.g., Ref. [24]. For finite interaction strengths, the behavior of the entropies above the quantum phase transition is more complex, corresponding to the various phases of the t - t' - U model²⁴.

C. Density-density interactions

We now turn to the effect of the interaction terms in the transformed Hubbard model (2). We start with the analysis of the density-terms $\hat{H}_{U,d}$ in (6), as shown in Fig. 3 (b). We neglect all other interaction terms and keep the single-particle hopping only, as shown in Fig. 3 (a), i.e., we analyze $\hat{H}_d = -\hat{H}_T + U\hat{H}_{U,d}$.

As seen from Fig. 13, the site entropy, the block entropy and the Schmidt number do not change significantly as a function of U . Instead, they mildly decrease as the interaction gradually eliminates double occupancies (and holes) from the Hilbert space. For small interaction strengths, the block entropy and the Schmidt number are fairly small. This is in accord with our observations for the Hubbard model with open boundary conditions. Obviously, purely local density-type interactions do not open new quantum channels and, therefore, they do not substantial increase the entanglement between blocks. Density-density interactions between different lattice sites behave qualitatively the same because they do not involve the exchange of particles between the blocks. Therefore, the DMRG still performs well for the Hubbard model with long-range density-density interactions when open boundary conditions are applied.

The situation changes when we treat the pair-hopping term $\hat{H}_{U,p}$ (6), shown in Fig. 3 (c), together with the kinetic energy \hat{H}_T . We ignore all other interaction terms, i.e., we treat $\hat{H}_p = -\hat{H}_T + U\hat{H}_{U,p}$ in Fig. 14. Again, the site entropy, the block entropy and the Schmidt number decrease smoothly as a function of the interaction strength. In comparison with the purely local interaction $\hat{H}_{U,d}$ the Schmidt number has almost doubled.

The increase in block entropy and Schmidt number is very similar when we study the effect of the spin-flip term $\hat{H}_{U,s}$ in (6), as shown in Fig. 3 (d). The result of the analysis of $\hat{H}_s = -\hat{H}_T + U\hat{H}_{U,s}$ is shown in Fig. 15. Apparently, the spin exchange between neighboring sites

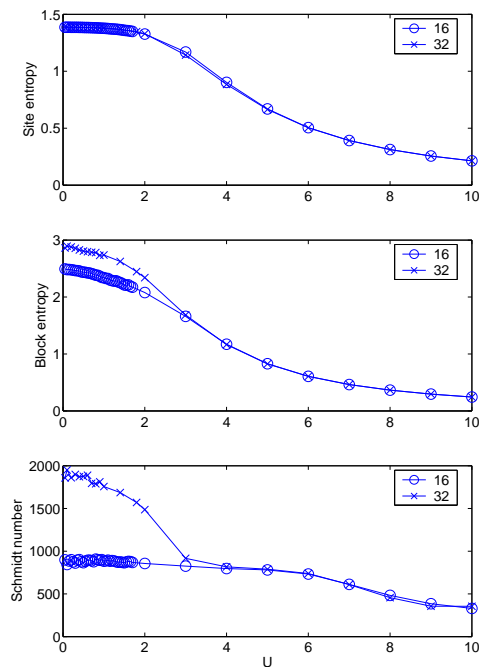


FIG. 13: Same as Fig. 11 but as a function of U for the local-density term only, $\hat{H}_d = -\hat{H}_T + U\hat{H}_{U,d}$, as shown in Fig. 3 (b).

creates entanglement similar to the exchange of pairs. In comparison of the effect of $\hat{H}_{U,d}$ on the one-hand side and $\hat{H}_{U,p}$, $\hat{H}_{U,s}$ on the other we conclude that not only the number of links and their strength but also the type of coupling plays an important role for the entanglement.

D. Super-site representation

Originally, as shown in Fig. 2, the transformed Hubbard model (2) is defined on a two-chain geometry with purely local interaction and electron transfers between neighboring sites. One may wonder whether the analysis of subsection V C is adequate because it is based on the single-chain geometry of Fig. 3.

In order to clarify this issue, we reduce the number of quantum channels between the DMRG blocks by forming ‘super-sites’ from lattice sites of type a and b . In this representation a lattice with $L_s/2 - 1$ sites and $q = 16$ degrees of freedom per site is formed, plus two end sites with $q = 4$ degrees of freedom, and open boundary conditions apply.

The two sites at the boundaries have the same site entropy for both models. In the super-site representation we halve the length of the system so that sites in the interior of the chain carry an entropy which is twice as large as for sites in the Hubbard model with periodic boundary conditions. A comparison of the block entropies is only meaningful for blocks which contain the same number of sites, i.e., $l = 3, 5, 7$ in Fig. 16. As expected, for

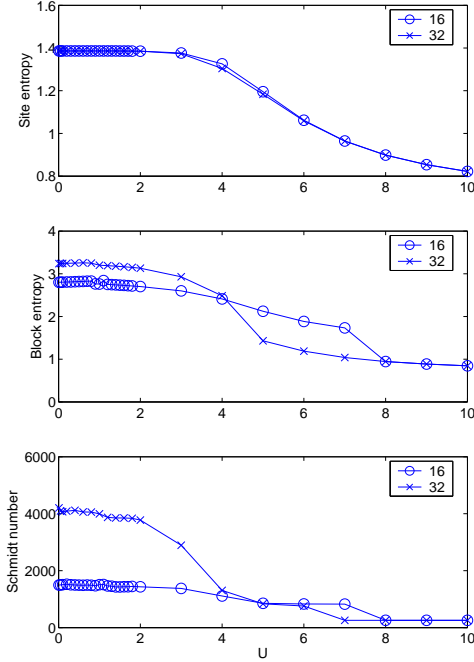


FIG. 14: Same as Fig. 11 but as a function of U for the pair-hopping term only, $\hat{H}_p = -\hat{H}_T + U\hat{H}_{U,p}$, as shown in Fig. 3 (c).

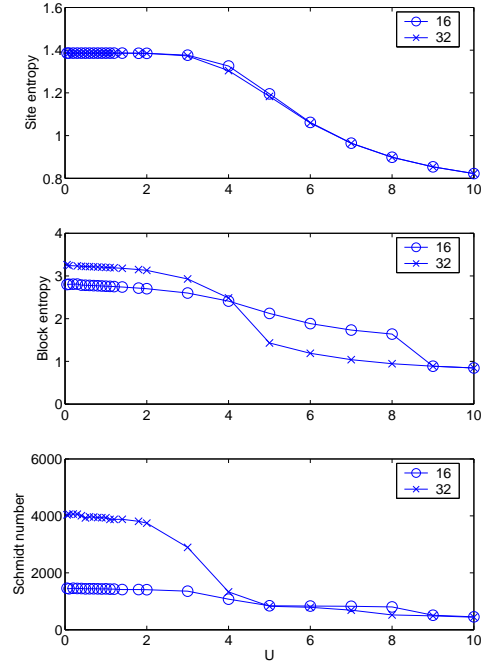


FIG. 15: Same as Fig. 11 but as a function of U for the pair-hopping term only, $\hat{H}_s = -\hat{H}_T + U\hat{H}_{U,s}$, as shown in Fig. 3 (d).

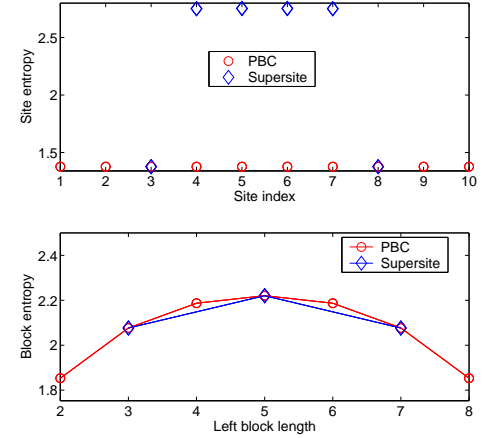


FIG. 16: Site entropy and block entropy for the half-filled Hubbard model for periodic boundary conditions shown in Fig. 5 (a) and for the super-site representation in Fig. 2 for $U = 1$ and $\chi = 0$ (exact calculation).

these block lengths they agree for both models. The total quantum information is essentially the same for both configurations. This observation is again readily explained by the fact that there are two quantum channels between the DMRG blocks in both representations. This is shown explicitly in Fig. 17 for $U = 0$ and $N = 34$, $\chi = 10^{-4}$ using maximum $M = 350$ block states.

The advantage that the transformed Hubbard model in the super-site representation is only of length $L_s/2 + 1$ is more than compensated by the fact that during the

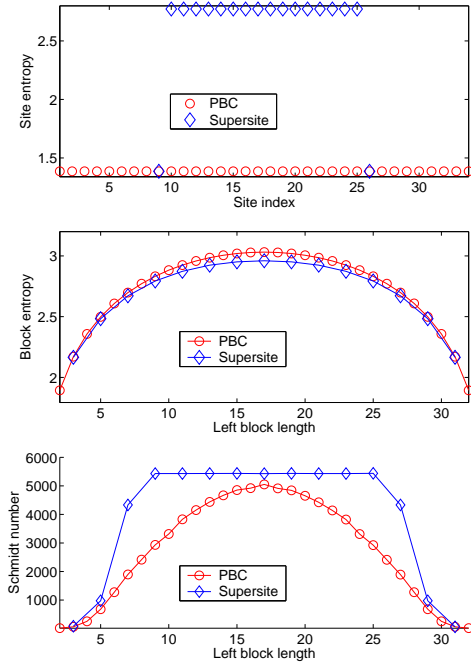


FIG. 17: Same as Fig. 16 for $U = 0$ for $N = 34$, $\chi = 10^{-4}$.

numerical calculation there are $q = 16$ degrees of freedom for the two intermediate sites s_l and s_r in the superblock representation. This higher demand for computational resources can be reduced if instead of two intermediate sites in the superblock representation only a single site is used. The modification of the DMRG in this direction is possible^{21,25}.

VI. CONCLUSIONS

We have constructed a unitary transformation between basis states for the one-dimensional Hubbard model sub-

ject to periodic boundary conditions so that open boundary conditions apply for the transformed Hamiltonian. Despite the fact that the one-particle and two-particle interaction matrices link nearest and next-nearest neighbors only, the performance of the density-matrix renormalization group method for the transformed Hamiltonian does not improve significantly because some of the new interactions act as independent quantum channels which generate the same level of entanglement as periodic boundary conditions in the original formulation of the Hubbard model.

The total quantum correlation in the system for the transformed model decreases only for small interaction strengths and for very short chain lengths. Therefore, this approach cannot be used to improve the performance of the DMRG for reasonable system sizes. We have shown that the localization of interactions alone does not improve the performance of the DMRG. Instead, it is affected more significantly by the number and the strength of the various quantum channels between the DMRG blocks.

In conclusion, our results contribute to a better understanding of the entanglement production within the DMRG. We propose to implement the communication length for the construction of an optimal basis and the proper ordering of lattice sites. The expected reduction of the block entanglement should improve the performance of the DMRG for Hamiltonians with long-range electron transfers and interactions.

Acknowledgments

This research was supported in part by the Hungarian Research Fund (OTKA) Grants No. T 043330 and F 046356. The authors acknowledge computational support from Dynaflex Ltd. under Grant No. IgB-32. Örs Legeza was also supported by a János Bolyai Research Scholarship.

- ¹ S.R. White, Phys. Rev. Lett. **69**, 2863 (1992); Phys. Rev. B **48**, 10345 (1993).
- ² T. Xiang, Phys. Rev. B **53**, 10445 (1996).
- ³ S. Nishimoto, E. Jeckelmann, F. Gebhard, and R.M. Noack, Phys. Rev. B **65**, 165114 (2002).
- ⁴ Ö. Legeza and J. Sólyom, Phys. Rev. B **68**, 195116 (2003).
- ⁵ S.R. White and R.L. Martin, J. Chem. Phys. **110**, 4127 (1998); S. Daul, I. Ciofini, C. Daul, and S.R. White, Int. J. Quantum Chem. **79**, 331 (2000).
- ⁶ G.K.-L. Chan and M. Head-Gordon, J. Chem. Phys. **116**, 4462 (2002).
- ⁷ A.O. Mitrushenkov, G. Fano, F. Ortolani, R. Linguerri, and P. Palmieri, J. Chem. Phys. **115**, 6815 (2001).
- ⁸ Ö. Legeza, J. Röder, and B.A. Hess, Phys. Rev. B **67**, 125114 (2003).
- ⁹ G.K.-L. Chan and M. Head-Gordon, J. Chem. Phys. **118**, 8551 (2003).

- ¹⁰ Ö. Legeza, J. Röder, and B.A. Hess, Mol. Phys. **101**, 2019 (2003).
- ¹¹ R.M. Noack and S.R. White in *Density Matrix Renormalization: A New Numerical Method in Physics*, ed. by I. Peschel, X. Wang, M. Kaulke, and K. Hallberg (Springer, Berlin, 1999), p. 27.
- ¹² J. Dukelsky and S. Pittel, Rep. Prog. Phys. **67**, 513 (2004).
- ¹³ U. Schollwöck, Rev. Mod. Phys. **77**, 259 (2005).
- ¹⁴ R.M. Noack and S.R. Manmana in *Lectures on the physics of highly correlated electron systems IX*, ed. by A. Avella and F. Mancini (AIP Conference proceedings **789**, Melville, New York, 2005), p. 93.
- ¹⁵ E. Cuthill and J. McKee in *Proceedings of the 24th National Conference of the Association for Computing Machinery* (ACM Press, New York, 1969), p. 157.
- ¹⁶ Ö. Legeza and J. Sólyom, Phys. Rev. B **70**, 205118 (2004).
- ¹⁷ J. Vidal, G. Palacios, and R. Mosseri, Phys. Rev. A **69**,

- 022107 (2004).
- ¹⁸ H. Fan, V. Korepin, and V. Roychowdhury, Phys. Rev. Lett. **93**, 227203 (2004).
- ¹⁹ J. Rissler, R.M. Noack, and S.R. White, unpublished (cond-mat/0508524, 2005).
- ²⁰ G. Moritz, B.A. Hess, M. Reiher, J. Chem. Phys. **122**, 024107 (2005).
- ²¹ F. Verstraete, D. Porras, and J.I. Cirac, Phys. Rev. Lett. **93**, 227205 (2004).
- ²² Ö. Legeza and J. Sólyom, (unpublished, 2005).
- ²³ For a review, see F.H.L. Essler, H. Frahm, F. Göhmann, A. Klümper, and V.E. Korepin, *The one-dimensional Hubbard model* (Cambridge University Press, Cambridge, 2005).
- ²⁴ G.I. Japaridze, R.M. Noack, and D. Baeriswyl (unpublished, 2005).
- ²⁵ S.R. White, unpublished (cond-mat/0508709, 2005).